Cite this: DOI: 10.1039/c0xx00000x

www.rsc.org/xxxxxx

ARTICLE TYPE

Micellar Drug Nanocarriers and Biomembranes: How do they Interact?

Antonio De Nicola,[a,b] Samira Hezaveh,[c] Ying Zhao,[d] Toshihiro Kawakatsu,[e] Danilo Roccatano,[c] and Giuseppe Milano,*[a,b]

Received (in XXX, XXX) Xth XXXXXXXXX 20XX, Accepted Xth XXXXXXXXX 20XX

DOI: 10.1039/b000000x

Pluronics based formulations are among the most successful nanomedicines and block-copolymer micelles including drugs are undergoing phase I/II studies as anticancer agents. Using coarse-grained models, molecular dynamics simulations of large-scale systems, modeling Pluronic micelles interacting with DPPC lipid bilayers, on the μs timescale have been performed. Simulations show, in agreement with experiments, a release of Pluronic chains from the micelle to the bilayer. This release changes the size of the micelle. Moreover, the presence of drug molecules inside the core of the micelle has a strong influence on this process. The picture emerging from the simulations is that the micelle stability is a result of an interplay between drug/micelle core and block-copolymer/bilayer interactions. The equilibrium size of the drug vector shows a strong dependency on the hydrophobicity of the drug molecules embedded into the core of the micelle. In particular, the radius of the micelle shows an abrupt increase in a very narrow range of drug molecule hydrophobicity.

Introduction

In medicine the use of nanosized tools for the diagnosis, prevention and treatment of diseases is becoming more and more popular.[1] First generation nanomedicines, nowadays, are in routine clinical use and include both "blockbuster" drugs and certain specific products.[2] In this context the use of polymeric materials is very broad[3] and polymer based formulations are among the most successful nanomedicines.[3-7]

Among several diseases, cancer is a major target of the development of new drugs with many clinical trials ongoing and involving nanomedicines.[8] Technologies include liposomes,[9-11] polymer conjugates[3-5] and block copolymer micelles.[6-7, 12-13] Tumor angiogenesis creates the gateway for tumor access of nanosized objects. Matsumura and Maeda described the enhanced permeability and retention (EPR) effect in the 1980s,[14] the "gaps" created by angiogenesis can be much larger (100 nm to 2 μm) than those reported in normal tissues. For this main reason, nanosized drugs tend to accumulate in tumor tissue much more than they do in normal tissues. Due to EPR effect, for these drug vectors, it is clear that the size of the drug carrier plays an important role. In fact, constructs in the size range of 5-30 nm are considered optimal, and thus the control of the size of systems for drug delivery is a key point.

Block copolymer micelles including drugs by physical entrapment are undergoing phase I/II studies as anticancer agents.[1] Pluronics as micellar aggregates have been employed to store several drugs,[15-18] where Pluronics are amphiphilic linear triblock copolymers having the central block of hydrophobic polypropylene oxide (PPO) covalently bonded with two blocks of hydrophilic polyethylene oxide (PEO). One example of successful application of Pluronics is the doxorubicin formulation SP1049C developed using a combination of two Pluronics, L61 and F127.[19]

Despite the large interest in Pluronics block copolymers for cancer therapy, only recently they became the subject of molecular simulation studies involving biomembranes.[20-25] The understanding of the interaction mechanisms of these synthetic polymers with biomembranes would need a description at atomic level of both structure and dynamics of the systems. Atomistic models can provide very accurate descriptions by using suitable force fields and they are potentially able to give consistent information. Such kind of models suitable for Pluronics have been proposed and validated in water and several solvents.[26-28] These models have been used to study the percolation and distribution of PEO chains using steered molecular dynamics, PEO and PPO oligomers[20,23] and Pluronics inside model biomembranes.[21-22] So far, none of these simulation studies have been addressed to understand the mechanism of interaction of Pluronics self-assembled structures like micelles with models of cell membranes. These studies are difficult because they involve the simulation of systems on length and time scales not accessible by atomistic simulation methods. To this aim, specific coarse-grained models that are able to keep molecular specificity can be used in order to reach time and length scales relevant for these systems. The dynamics of these processes at molecular level is so far that also the experimental measurements cannot easily accessible and therefore many questions are still undisclosed on the molecular details of the interaction mechanisms.

In this paper, we report the development and validation of coarse-grained models of Pluronics that are able to describe micellar assemblies and their interactions with phospholipids. Furthermore, we employ these models for large-scale simulations of Pluronic L64 micelles interacting with

dipalmitoylphosphatidylcholine (DPPC) lipid bilayers. Due to the relevance of these block-copolymers, assembled nanostructures for drug delivery applications, the role of embedded drug molecules has been also considered. In particular, we focused on the interplay between the interactions of drug molecules with the hydrophobic core of the micelle and their mutual influence on the micelle stability in the presence of lipid bilayer structures.

Models and Method

Simulation Methodology

The coarse-grained (CG) models considered in this work have been developed in a hybrid particle-field (PF) scheme combining particles with a field representation for non-bonded interactions.

Hybrid models, due to their computational efficiency, are gaining popularity for simulations of several soft matter systems including nanocomposites[29] and biomembranes.[30-31] For example, a solvent-free coarse-grained model for lipid bilayer membranes where nonbonded interactions were treated by a weighted-density functional has been introduced by Hömberg and Müller.[32] Very recently, Sevink et al.[33] introduced a hybrid scheme, combining Brownian dynamics (BD) and dynamic density functional theory (DDFT), that is able to model efficiently complete vesicles with molecular detail.

Particle and field representation of coarse-grained models has been considered in the single chain in mean field (SCMF) method and has been applied to homopolymer and block copolymer systems as reported by Muller *et al*.[34-35] More recently, the Molecular Dynamic (MD) method has been combined with self-consistent field (SCF) description, which hereafter we call "MD-SCF" approach. In particular, an implementation suitable for the treatment of atomistic force fields and/or specific CG models has been reported and validated.[36-37]

The main feature of the MD-SCF approach, is that the evaluation of non-bonded forces and the potential between atoms of different molecules is replaced by the evaluation of a potential dependent on the local density at position **r**. According to SCF theory, a many body problem like molecular motion in a many-molecule system is reduced to the derivation of a partition function of a single molecule in an external potential $V(\mathbf{r})$. Then, forces between non-bonded particles can be obtained from a suitable expression of the $V(\mathbf{r})$ and its derivatives.

In the framework of SCF theory, a molecule is considered to be interacting with the neighbouring molecules only through a mean field. To derive such a mean-field picture, we split the Hamiltonian of our target system, composed of M molecules, into two parts:

$$\hat{H}\left(\Gamma\right) = \hat{H}_0\left(\Gamma\right) + \hat{W}\left(\Gamma\right), \qquad (1)$$

where Γ specifies a point in the phase space, which is used as shorthand for a set of positions of all atoms in the system. Moreover, we denote with the symbol ^ (hat) that the associated physical quantity is a function of the microscopic states described by the phase space Γ.

The term $\hat{H}_0\left(\Gamma\right)$ is the Hamiltonian of a reference system composed of non-interacting molecules including all the intramolecular interaction terms (bond, angle, etc.) that are usually considered in MD simulations. The term $\hat{W}\left(\Gamma\right)$ is the deviation from the reference system due to non-bonded interactions.

The partition function of the system, assuming the canonical (NVT) ensemble, is given by:

$$Z = \frac{1}{M!}\int d\Gamma \exp\left\{-\beta\left[\hat{H}_0\left(\Gamma\right) + \hat{W}\left(\Gamma\right)\right]\right\}, \qquad (2)$$

where: $\beta = \frac{1}{k_B T}$

From a microscopic point of view, the number density of segments can be defined as a sum of delta functions placed at the center of mass of each particle as[36]:

$$\hat{\phi}\left(\mathbf{r};\Gamma\right) = \sum_{p=1}^{M}\sum_{i=0}^{S(p)}\delta\left(\mathbf{r} - \mathbf{r}_i^{(p)}\right), \qquad (3)$$

where $S(p)$ is the number of particles contained in p-th molecule, $\mathbf{r}_i^{(p)}$ is the position of the i-th particle in p-th molecule.

The calculation of the interaction term $\hat{W}(\Gamma)$ is done by introducing several assumptions. The first assumption is that $\hat{W}(\Gamma)$ depends on Γ only through the segment number density $\hat{\phi}\left(\mathbf{r};\Gamma\right)$ as:

$$\hat{W}\left(\Gamma\right) = W\left[\hat{\phi}\left(\mathbf{r};\Gamma\right)\right], \qquad (4)$$

where $W\left[\hat{\phi}\left(\mathbf{r};\Gamma\right)\right]$ means that W is a functional of $\hat{\phi}\left(\mathbf{r};\Gamma\right)$. Using the assumption of Eq.4 together with the definition of δ-functional

$$\delta\left[\hat{\phi}\left(\mathbf{r};\Gamma\right) - \phi\left(\mathbf{r}\right)\right] = \int D\left\{w\left(\mathbf{r}\right)\right\}\exp\left[i\int w\left(\mathbf{r}\right)\left\{\hat{\phi}\left(\mathbf{r};\Gamma\right) - \phi\left(\mathbf{r}\right)\right\}d\mathbf{r}\right], \qquad (5)$$

the partition function of the system, in Eq. 2, can be rewritten as:

$$Z = \frac{1}{M!}\int D\{\phi(\mathbf{r})\}\int D\{w(\mathbf{r})\exp\{-\beta[-\frac{M}{\beta}\ln z + W[\phi(\mathbf{r})] - \frac{1}{i\beta}\int w(\mathbf{r})\phi(\mathbf{r})d\mathbf{r}]\}, \qquad (6)$$

where z is the single molecule partition function in an external field, $w(\mathbf{r})$ is a conjugate field of $\phi\left(\mathbf{r}\right)$ which appeared in the Fourier representation of the δ-functional, and is a complex field.

The mean field approximation, in terms of partition function, is obtained by replacing the integrals over $w(\mathbf{r})$ and $\phi\left(\mathbf{r}\right)$ in Eq.6 with a Gaussian integral around the most probable state that

minimizes the argument of the exponential function on the right-hand side of Eq.6 (so-called saddle point approximation).

The minimization conditions obtained by functional derivatives are:

$$\begin{cases} V(\mathbf{r}) \equiv \dfrac{1}{i\beta} w(\mathbf{r}) = \dfrac{\delta W[\phi(\mathbf{r})]}{\delta \phi(\mathbf{r})} \\ \phi(\mathbf{r}) = -\dfrac{M}{\beta z} \dfrac{\delta z}{\delta V(\mathbf{r})} = \langle \hat{\phi}(\mathbf{r};\Gamma) \rangle \end{cases}, \quad (7)$$

where $\phi(\mathbf{r})$ is the coarse-grained density at position $\mathbf{r}$ and $V(\mathbf{r})$ is the external potential conjugate to $\phi(\mathbf{r})$ which is a real field.

In term of Eq. 7, it is possible to obtain an expression for the external potential acting on each particle. Next, we assume that the density dependent interaction potential W, where each component species is specified by the index K, has the following form:

$$W[\{\phi_K(\mathbf{r})\}] = \int d\mathbf{r} \left(\frac{k_B T}{2} \sum_{KK'} \chi_{KK'} \phi_K(\mathbf{r}) \phi_{K'}(\mathbf{r}) + \frac{1}{2\kappa} \left(\sum_K \phi_K(\mathbf{r}) - 1 \right)^2 \right), \quad (8)$$

where $\phi_K(\mathbf{r})$ is the coarse-grained density of the species K at position $\mathbf{r}$ and $\chi_{KK'}$ are the mean field parameters for the interaction of a particle of type K with the density fields due to particles of type K'. Here we redefined $\phi_K(\mathbf{r})$ as the number density of the species K normalized by the total average number density of the particles. This change in the definition of $\phi_K(\mathbf{r})$ only affects the scale of the conjugate field $V(\mathbf{r})$.

The second term of the integrand on the right-hand side of eq. 8 is the relaxed incompressibility condition, where κ is the compressibility that is assumed to be sufficiently small (for the systems considered in this paper the value of 1/κ is 10 kJ/mol) .[36] Then, the corresponding mean field potential is:

$$V_K(\mathbf{r}) = \frac{\delta W[\{\phi_K(\mathbf{r})\}]}{\delta \phi_K(\mathbf{r})} = k_B T \sum_{K'} \chi_{KK'} \phi_{K'}(\mathbf{r}) + \frac{1}{\kappa} \left(\sum_K \phi_K(\mathbf{r}) - 1 \right). \quad (9)$$

In the case of a mixture of two components A and B as an example, the mean field potential acting on a particle of type A at position $\mathbf{r}$ is given by:

$$V_A(\mathbf{r}) = k_B T \left[\chi_{AA} \phi_A(\mathbf{r}) + \chi_{AB} \phi_B(\mathbf{r}) \right] + \frac{1}{\kappa} \left(\phi_A(\mathbf{r}) + \phi_B(\mathbf{r}) - 1 \right). \quad (10)$$

Thus, the force acting on the particle A at position $\mathbf{r}$ imposed by the interaction with the density field is

$$F_A(\mathbf{r}) = -\frac{\partial V_A(\mathbf{r})}{\partial \mathbf{r}} = -k_B T \left(\chi_{AA} \frac{\partial \phi_A(\mathbf{r})}{\partial \mathbf{r}} + \chi_{AB} \frac{\partial \phi_B(\mathbf{r})}{\partial \mathbf{r}} \right) - \frac{1}{\kappa} \left(\frac{\partial \phi_A(\mathbf{r})}{\partial \mathbf{r}} + \frac{\partial \phi_B(\mathbf{r})}{\partial \mathbf{r}} \right). \quad (11)$$

The main advantage of hybrid MD-SCF scheme is that the most computationally expensive part of the MD simulations, the calculation of the non-bonded forces, is replaced by the evaluation of forces between single particles with external potentials. In order to connect particle and field models, for the proposed hybrid MD-SCF scheme, it is necessary to obtain a smooth coarse-grained density function directly from the particle position Γ. Let us denote this procedure as

$$\bar{S}\{\hat{\phi}(\mathbf{r};\Gamma)\} = \phi(\mathbf{r}), \quad (12)$$

where $\bar{S}$ is a symbolic name of the mapping from the particle positions to the coarse-grained density $\phi(\mathbf{r})$. This density field is obtained by dividing the simulation box into several sub-cells. Then, according to the position of each particle inside a cell, a fraction of the particle is assigned to each vertex of the cell. In order to explain such procedure, a two-dimensional case is schematized in Figure 1A.

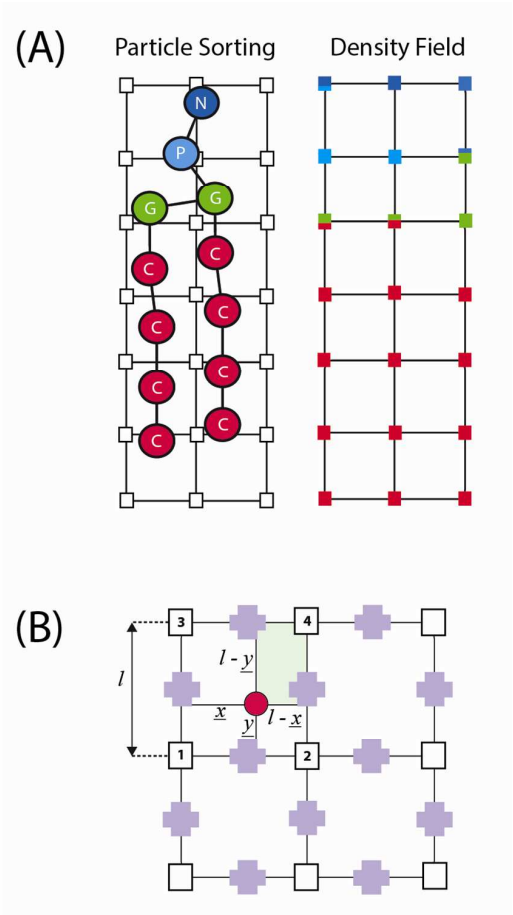

Fig.1 (A) Assignment of coarse-grained density to the lattice points for a phospholipid. (B) Criterion for assignment to a particle fraction to lattice points.

As shown in Figure 1B, the fraction of a particle assigned to a given lattice point is proportional to the area of a rectangle showed in the figure. According to the procedure described above, the size of the cell l is a spatial parameter defining the extent of density coarse-graining. Larger is the value of l, more particles will be included in each cell and coarser is the calculated density. Once the coarse-grained density has been calculated from particle positions, the spatial derivatives of the density fields can be evaluated. The iteration algorithm used in MD-SCF approach is the following: According to the initial configurations

of the system (at time t_0), a starting value of the coarse-grained density is obtained and density gradients at the particles positions are calculated by linear interpolation. Then, from the density gradients, forces acting on the particles at position **r** due to the interaction with the density fields are computed according to Eq. 11. The total force acting on the particles will be the sum of the intramolecular forces (bonds, angles, etc. calculated as in classical MD simulations) and the forces due to the interactions of particles with density fields. After the force calculation, a new configuration is obtained by integration of the equation of motion.

It is worth noting that, for these models the use of mean field does not correspond to a truly field-based method or just particle–field coexistence. The density field remains a close function of particle coordinates, and is not an independent variable in the free energy functional. According to the instantaneous field approximation discussed by Doulas *et al*. in the framework of SCMF Monte Carlo simulations,[34] it is possible to tune a time interval to update the density field without loss of accuracy. The main assumption is that the field, as collective variable with respect to particle coordinates, has a slow change with respect to particles displacements in one or more timesteps. The optimal value of updating frequency (Δt_{update}) depends on the resolution of the density (i.e. the size of the sub-cell where the particles are grouped), the system nature and its conditions. For the systems considered here and reported in references [36-40] we found that the value of Δt_{update} of starting from 600 to lower values of time steps gives enough accurate results.

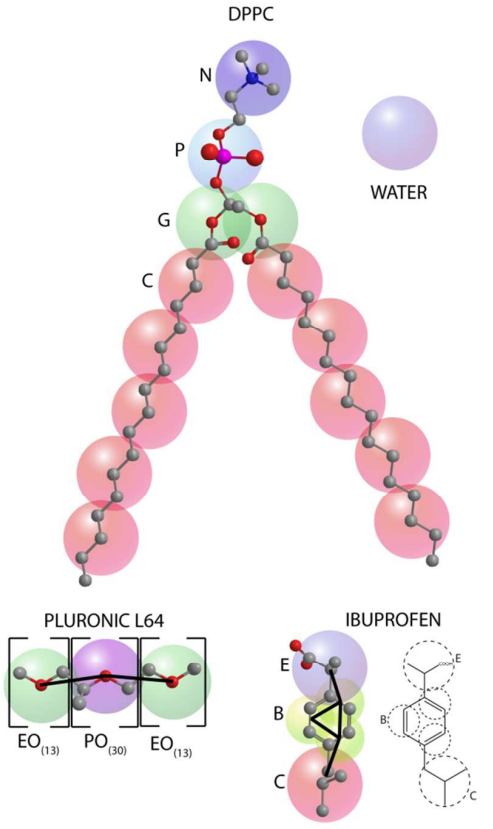

Fig.2 Mapping scheme adopted for the models considered in this paper.

Simulation Details

Simulations reported here have been performed using the parallelized version of the OCCAM code.[41]

All simulations have been performed with velocity Verlet algorithm using a time steep of 0.03 ps in the *NVT* ensemble by keeping the temperature constant at 325 K using Andersen thermostat with a collision frequency of 7 ps^{-1}. The calculation of the fields have been performed using a grid resolution of 0.705 nm and an update frequency (Δt_{update}) of 300 steps.

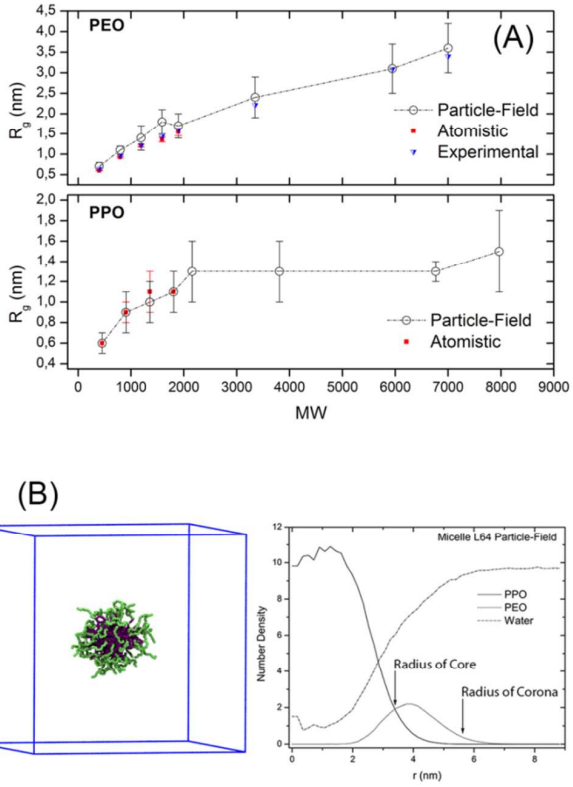

Fig.3 (A) Radius of gyration vs. molecular weight for PEO (upper) and PPO (bottom) chains in water. In the plots values obtained from atomistic (red squares), experiments (blue triangles) and coarse-grained MD-SCF models (empty circles) are compared. (B) Radial density profile calculated for a L64 micelle (system I) after 4.5 μs of MD-SCF simulation. Arrows indicate experimental values of core and corona radii.

Models and Parameters

The coarse-grained models adopted in this study for lipids have been extensively described and validated in two previous papers.[38-39] These models suitable for modelling biomembranes have been recently reviewed[31]. For the models used in this work for Pluronics, intramolecular bonded interactions, bond and angle potentials have been taken from the ones reported in reference[25] while non-bonded interactions are described using a field theoretic approach.

The parametrization of the MD-SCF models suitable for Pluronics has been done considering different reference systems. Models of PEO and PPO chains have been developed considering effective particles, centered at the oxygen atoms, each of them grouping the atoms of one repeating unit. The mapping scheme adopted in this work is depicted in Figure 2. The scheme can be considered as a 3:1 mapping for PEO and 4:1 mapping for PPO, i.e. three (for the EO unit) and four (for the PO unit) non-hydrogen atoms are grouped into one bead.

Bonds are described by a harmonic potential of the form:

$$V_{bond}(l) = \frac{1}{2}K_{bond}(l - l_0)^2, \qquad (11)$$

where l_0 is the equilibrium bond length and K_{bond} is the force constant. Parameters for all bond types are reported in Table 1.

The stiffness of the chains is also taken into account by a bending potential $V_{\mathrm{angle}}(\theta)$ that depends on the cosine of the angle θ between two successive bonds.

$$V_{angle}(\theta) = \frac{1}{2}K_{angle}\left\{\cos(\theta) - \cos(\theta_0)\right\}^2, \qquad (12)$$

where K_{angle} is the force constant and θ_0 is the equilibrium bond angle. Parameters adopted for all angle types are reported in Table 2.

According to Eq. 9, in order to calculate the MD-SCF potential, several mean field parameters $\chi_{KK'}$ between a particle of type K with the density field due to particles of type K' are needed. In Table 3 the set of $\chi_{KK'}$ parameters used in this study are reported. Models of lipid bilayers have been fully validated in references 38 and 39. Mean field $\chi_{KK'}$ parameters for the interaction of ethylene oxide (EO) and propylene oxide (PO) repeating units with water and lipid bilayers have been tuned to reproduce several reference data from atomistic simulations.[23] Further details about the parametrization will be given in the following.

Results and Discussion

L64 Single Chains and Micelle in water

Mean field interaction parameters ($\chi_{KK'}$ of eq. 9, given in Table 3) between EO and PO beads and water have been tuned to reproduce the behavior of the gyration radius with respect to the chain length obtained from atomistic simulations. An initial set of parameters for the interaction of EO and PO with water ($\chi_{\mathrm{PEO,W}} \times RT = 2.1$ and $\chi_{\mathrm{PPO,W}} \times RT = 3.4$ kJ/mol) has been derived from a_{ij} parameters used in Dissipative Particle Dynamics (DPD) models reported by Cao et al.[42] and using the linear relation introduced by Groot and Warren[43] connecting χ and a (χ=0.286 Δa). These initial values have been adjusted to the values reported in Table 3 to reproduce chain dimensions obtained from atomistic simulations of PEO and PPO single chains in water. In Figure 3A values of radius of gyration as for different molecular weights (MW) calculated using MD simulations of atomistic model and MD-SCF simulations of coarse-grained models of PEO and PPO are reported.

A validation of the proposed models for assembled chains has been done considering the size and the stability of micelles. In particular, the Pluronic L64 represented by the formula $(EO)_{13}$-$(PO)_{30}$-$(EO)_{13}$ has been considered. In Figure 3B, together with a snapshot of simulated system I of Table 6, the radial density profiles calculated for a L64 micelle having 38 block copolymer chains (corresponding to the experimental aggregation number) are reported. Experimental values of core and corona radius[44] are indicated by arrows in the plot. The radial density profiles of PO and EO blocks calculated from a simulation of system I (2.5 wt % of L64 in water) well compare with the experimental values of core and corona radii obtained in the same conditions.[44]

The critical micelle concentration (CMC) of the L64 model has been investigated considering the stability of the system as a function of L64 concentration. In particular, fractions of assembled L64 chains have been calculated for systems at different concentrations (Table 5). In Figure 4 the fraction of assembled L64 chains compared with the experimental value of the CMC are reported. A good agreement with the value of 0.344 mM reported by Alexandridis[45] has been obtained. Further validations on micelles behavior (aggregation number) are reported in the supporting information section. The Pluronics model reported here gives a correct reproduction of the occurrence of micellar and non-micellar phases for Pluronics L62 and L64 as function of water concentration. In particular, the proposed models are able to correctly describe the different morphologies (such us hexagonal micellar, lamellar and complex interconnected) that have been found experimentally.[40]

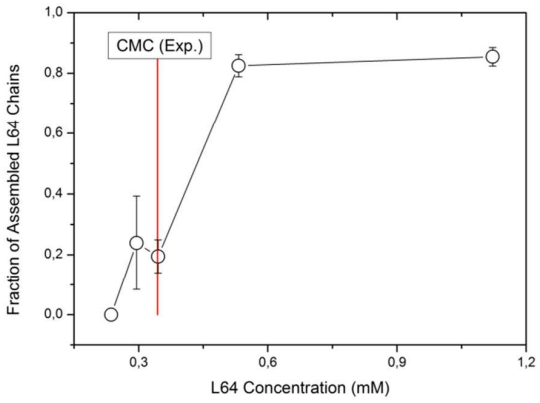

Fig.4 Fraction of assembled L64 chains at different concentrations, corresponding to the systems described in Table 5. Chains are counted as assembled if the number of neighboring chains is different from zero. The number of neighbors is calculated on the basis of a cut off criterion (1 nm) on the shorter distance between PO units of two different L64 chains. Each point in the plot corresponds to an average obtained from the last 100 ns of each simulation. The time behavior of the fraction of assembled chains for all the five systems are reported in the supporting information section.

Micelle in contact with DPPC bilayer

The parametrization of the interaction parameters $\chi_{\mathrm{KK'}}$ between EO and PO beads with phospholipids (Table 3) has been based on the reproduction of density profiles from reference atomistic simulations of PEO and PPO oligomers in contact with lipid bilayers.[24] An initial set of χ for EO and PO interactions with

lipids head and tail has been obtained from a systematic DPD study of Groot on polymer-surfactant systems. In particular, set 1 (according to the notation of ref 43) for EO/lipid head and EO/lipid tail and intermediate values between sets 6 and 7 for PO/lipid head and PO/lipid tail, have been chosen. Further slight adjustments of parameters have been done to better reproduce reference partial density profiles obtained from atomistic simulations. Density profiles and description of systems used for the parametrization are reported in Supporting Information Section.

According to the experimental data the diameter of the micelle is around 12 nm.[44] For this reason, in order to avoid large finite size effects, in the simulations reported here, a box size of 2.5 times larger than micelle diameter in the *x* and *y* directions (30 nm) and 2.8 in *z* direction (34 nm) has been employed. This implies simulations of quite large-scale systems having more than 250.000 particles (see Table 6).

In Figure 5A several snapshots of the MD simulation of system II made of one Pluronic L64 micelle in contact with a DPPC lipid bilayer are reported (water beads are not shown for clarity). The simulation performed on the μs scale reveals that the behavior of the polymeric micelle is strongly influenced by the presence of lipid bilayer. In particular, from the beginning of the simulation chains are released from the micelle to the water phase and starting from about 1 μs insertions of Pluronic triblock chains inside the bilayer can be observed. This behavior is in agreement with the experimental one reported by Pemboung et al.[46] In particular, ^{1}H-NMR and spin labeled probes results suggest a release of L64 chains inside dodecylphosphocoline (DPC) and DPPC micelles.

Simulations snapshots show that chains attach to the lipid bilayer inserting the hydrophobic segment made of PO beads in the hydrophobic portion of the bilayer. In Figure 5C a detail of an inserted L64 chain of system II is depicted. In agreement with the findings of Firestone et. al,[47-48] chains are inserted partially inside the bilayer with the PPO block, while the PEO blocks point toward the water phase from the same side of the lipid bilayer. The chain release process continues until the micelle dissolves in the water phase. This behavior can be ascribed to an effective concentration of L64 in the water phase lower than the CMC due to a subtraction of polymer chains from the micellar assembly and from water caused by the insertion inside lipid bilayer. From the plot of Figure 5B it is clear that in about 3 μs the L64 chains are unassembled with a fraction 0.2 present as free chains and the remaining L64 chains inserted inside the lipid bilayer.

Usually, for coarse-grained models the dynamics is faster than corresponding atomistic ones. This happens because there is a reduced effective bead friction due to smaller energy barriers and/or a smoother energy landscapes. In order to connect the results with less coarse models (atomistic or CG but

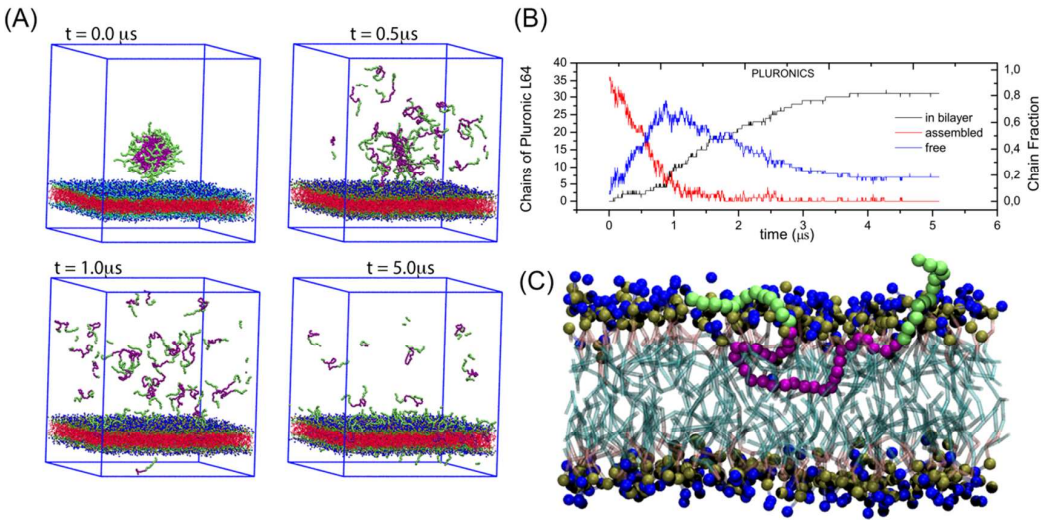

Fig.5 (A) Snapshots of system II (258.072 coarse-grained beads corresponding to ~ 3.000.000 of atoms) having a L64 micelle in contact with DPPC lipid bilayer (water beads are omitted for clarity) (B) Time behavior of L64 chains assembled as micelle (red curve), inside lipid bilayer (black curve) and in water (blue curve). L64 chains, for a given configuration, are counted as inside bilayer if at least one PO bead is located between the average heights of upper and lower lipid layers. The remaining chains are counted as free or assembled according to the number of neighboring chains (zero neighbors free chains, at least one neighbor assembled chains). The number of neighbors is calculated on the basis of a cut off value (1 nm) on the shortest distance between PO units of two different L64 chains. (C) Detail of insertion of a Pluronic L64 chain inside phospholipid bilayer. The green beads correspond to EO units, while the purple beads correspond to PO units. The aliphatic chains of phospholipids are shown in transparency. The head groups of DPPC are shown.

based on particle-particle potentials) or with experiments it is necessary to derive a scaling factor for the time.[49] Methods to match time scales can be applied to quantitatively understand and predict dynamics of several systems by coarse-grained models using a comparison between dynamical properties calculated at coarse-grained and atomistic levels. One possible way is the comparison between diffusion coefficients calculated from the coarse-grained and atomistic simulations. In the present case, from the comparison of diffusion coefficients a factor of about 15 can be obtained.[38] This simple comparison can give just an idea because the complication in soft matter systems is the multitude of energy barriers of similar height and a common problem is that usually all barriers are not lowered in the exact same way.

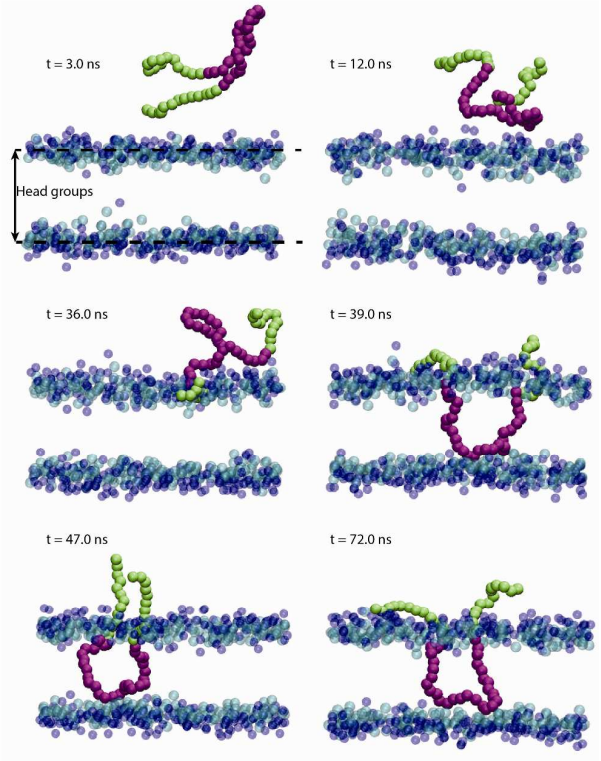

Fig.6 Snapshots of single L64 chain insertion process for an MD-SCF simulation. The insertion of PPO hydrophobic block is observed starting from 39 ns. The L64 chain after insertion shows the hydrophobic block inside the aliphatic region of phospholipid bilayer, while PEO blocks point toward the water phase from the same side.

In order to better define a scaling factor for the process of a chain insertion into a lipid bilayer, a closer timescale connection can be done comparing the time needed for an insertion of a single chain using MD-SCF and MD using traditional models based on Lennard-Jones pair potentials. Ideally, the exchange process of L64 chains between the micelle and the lipid bilayer, reported in the present paper, can be divided in three elementary processes. In particular, we can consider three processes: Pluronic chain detachment from the micelle, chain diffusion in water, chain insertion into the lipid bilayer. Reasonably, the diffusion process is the slowest one and it governs the rate of the observed process. In order to prove this, we performed three independent simulations similar to the one reported in Figure 6. In particular, we analyzed the velocity of L64 chain insertion from the time behavior of z component (perpendicular to the bilayer plane) of the distance between the geometric center of the PPO block and the hydrophobic sector of the lipid bilayer. According to this analysis, chain insertion is fast (takes about 8-10 ns) and it shows similar velocities for both particle-particle and particle field simulations. More details about this are reported in the supporting information section.

We can reasonably conclude that the slowest process governing the chain exchange between the micelle and the bilayer is the diffusion of L64 chains. In this way, a reasonable estimate of the order of magnitude of the scaling factor, for the observed process, could be the ratio between diffusion coefficients of particle-particle and particle-field simulations (a factor 15).

This feature allows to fully observe on the scale of our simulations the exchange of polymer chains between the micelle and the bilayer and the dissolution process of the micelle in presence of the lipid bilayer. Furthermore, equilibrium values of the distribution of L64 chains inserted into the bilayer and in water phase can be reached.

In absence of a lipid bilayer, we found that the micelle is stable. In particular, in Figure 7A, several snapshots of the MD simulation for 6 μs of a system having an L64 micelle in water (system I) are reported. Furthermore, the time behavior of radius of gyration of the micelle in water is reported in Figure 7B. Differently from system II the micelle is stable and an exchange of few chains between micelle and water phase is only observed.

In Figure 8A we report snapshots of system III, which is analogous to system II, but having four molecules of ibuprofene (IBU) encapsulated into the hydrophobic core of the micelle. In Figure 2 the mapping scheme used for IBU molecule together with its chemical structure is reported. In particular, the isopropyl group has been modeled by a bead of type C, the benzene ring using three beads of type B (having the same χ parameters of beads of type C) and the carboxylic group (COOH) with a bead of type E (having the same χ parameters of beads of type EO). Further details about intramolecular interactions (bonds and angles) of beads of types B and E are reported in Tables 1 and 2. The number of IBU molecules corresponds to 0.25wt% with respect to the quantity of L64. This value, as reported from Foster et al. is consistent with the aggregation number of 38 chains.[50]

Similarly to the previously described system II, after about 1μs (Figure 8B) the insertion of triblock chains into the bilayer takes place, but differently from the previous system II, although a reduction of micelle size is observed (Figure 8C), the micellar assembly is not dissolved. In particular, after 5 μs the micellar aggregate reaches its equilibrium size, and starting from 5 up to 9 μs only a slow repartition between chains in water and inside the bilayer occurs. After 9 μs up to the end of simulation (about 5 μs) the system remains in equilibrium state.

From these results it is clear that the hydrophobic nature of the encapsulated molecule influences the stability of the micellar assembly in the presence of a lipid bilayer. Small-angle neutron scattering and pulsed-field gradient stimulated-echo nuclear magnetic resonance (NMR) have shown that addition of hydrophobic molecules to solutions of Pluronics and water changes the micellar structure. In particular, high hydrophobic molecule concentrations favor micellization, leading to an increase of aggregation numbers, fraction of polymer micellized, and core radius of the micelle.[50] This behavior can be ascribed to the hydrophobic nature of the molecule encapsulated inside the micelle and the resulting favorable interactions with the micelle core.

In order to validate results based on a single simulation, we reported and compared the results of three different independent simulations for system III described above. In particular, comparisons between the behavior of block averages of the different simulations and the instantaneous time behavior of the three different states of Pluronic chains (free, assembled and inserted into the bilayer) show similar features. In particular, the main behavior in all three cases is very similar and at equilibrium the chain distributions converge to very close values. Due to their

similarity, we expect close behaviors in all considered systems. More information about this validation including plots and their comparison are reported in the supporting information section.

In our simulations the presence of the lipid bilayer changes the micelle aggregation state. In particular, in absence of IBU molecules, the 80% of L64 chains are inserted inside the DPPC bilayer. This causes a drop of L64 concentration in water phase and then a destabilization of micellar aggregate. In contrast, in the presence of hydrophobic IBU molecules, L64 chains are still assembled. This behavior shows a complex interplay between drug/micelle core and L64/bilayer interactions modulating the structural modifications of both micelle and bilayer. The main

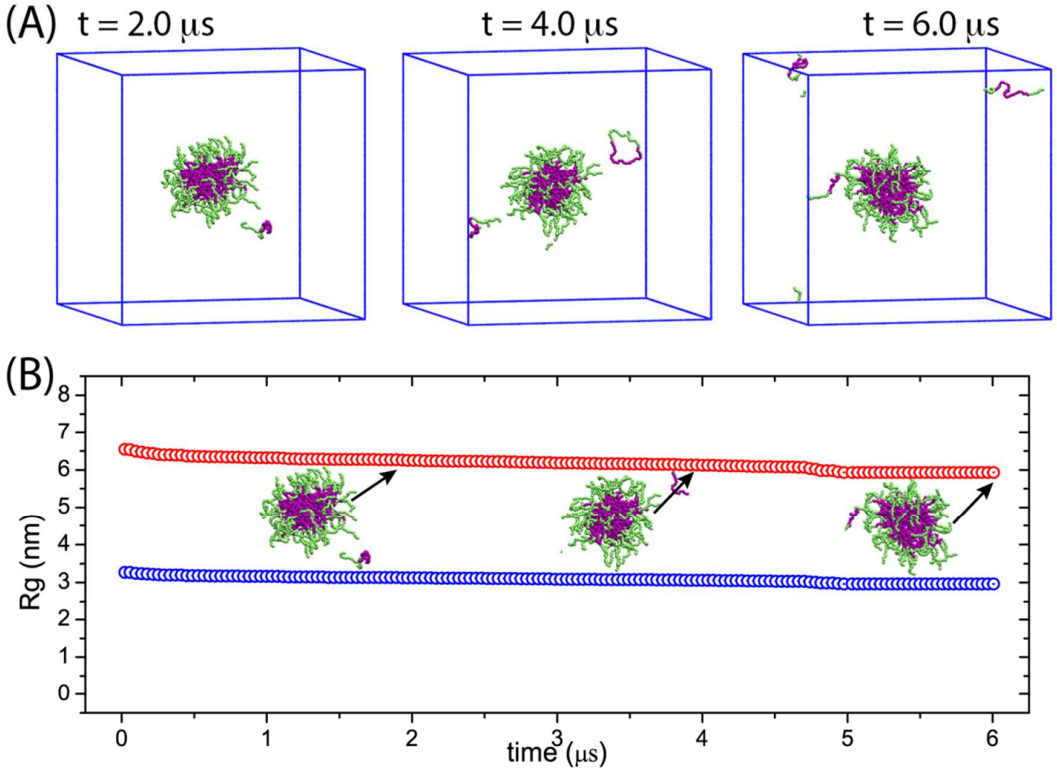

Fig.7 (A) Snapshots of system I having an L64 micelle in water (the beads of water are omitted for clarity). (B) Time behaviour of radius of gyration of L64 micelle in water. The red curve corresponds to the total radius of gyration of micelle while the blue curve corresponds to the radius of gyration of hydrophobic core. Snapshots of some configurations of the L64 micelle are shown at different times.

effect of the drug molecule seems to be related to its hydrophobicity.

With this in mind, further simulations aimed to study systematically this effect have been performed. In particular, trimers of increasing hydrophobicity have been included in the hydrophobic core of the L64 micelles. The number of trimers included in the micelle core is 8; this choice has been done to keep the number of particles similar to system III in which 5 IBU molecules (represented 5 by coarse-grained beads) have been included. The hydrophobicity of the trimers has been varied by changing linearly the χ parameters from the values assigned to the most hydrophobic particles (type C of lipid molecules) to those ones of water using a single parameter λ. In this way $\lambda = 1$ corresponds to a particle of type C and $\lambda = 0$ of a particle with the properties of water. For the intermediate cases, a linear combination has been used for all parameters. Simulations have been performed for seven different systems (IV-A to IV-G) having values of λ (0.16, 0.2, 0.5, 0.6, 0.8, 0.9, 1.0). In Table 4 the corresponding χ parameters for interaction between the beads of the trimers and the fields corresponding to the other particle types are reported.

In Figure 9 representative snapshots for some of these systems have been reported. For trimers having λ larger than 0.5 the micelles are stable during MD simulations. After 10 μs the

Cite this: DOI: 10.1039/c0xx00000x

www.rsc.org/xxxxxx

ARTICLE TYPE

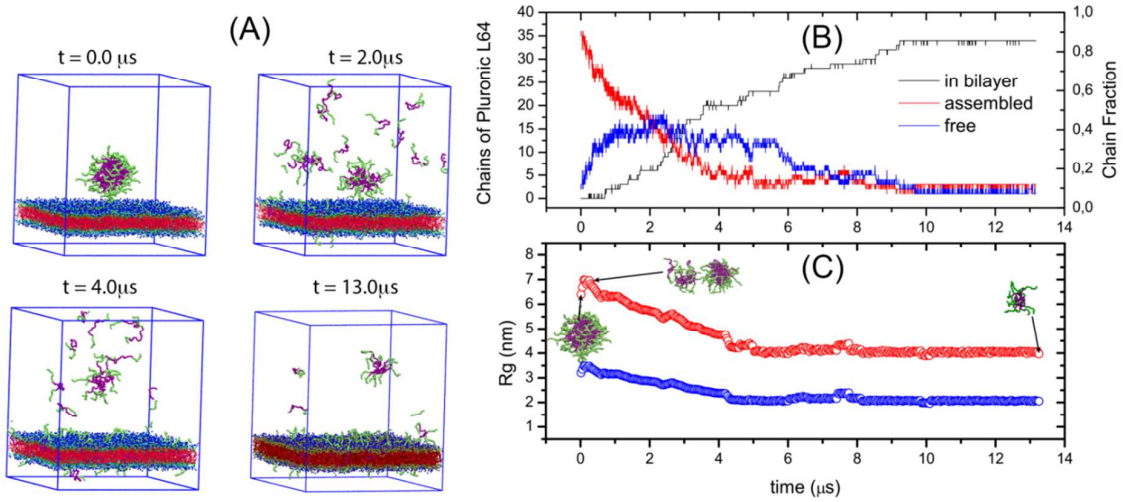

Fig.8 (A) Snapshots of system III (258.072 coarse-grained beads corresponding to ~3.000.000 of atoms) having an L64 micelle in contact with DPPC lipid bilayer (water beads are omitted for clarity) (B) Time behavior of L64 chains assembled as micelle (red curve), inside lipid bilayer (black curve) and in water (blue curve). For a complete definition of assembled, free and inside bilayer chains the reader can refer to the caption of **Figure 4**. (C) Time behavior of radius of gyration of L64 micelle with ibuprofen molecules embedded in the hydrophobic core. Red curve corresponds to the total radius of gyration of micelle while the blue curve corresponds to the radius of gyration of hydrophobic core. Snapshots of relevant configuration of L64 micelle are shown at different times.

micelle aggregate does not change and it still remains stable up to the end of simulation. The behavior observed for values of λ lower than 0.5 is very similar to the one obtained for an "empty" micelle. For lower values of λ (from 0.16 to 0.2) after about 10 ns all the inserted molecules diffuse out from the micelle and are stably present in the water phase. This is not surprising because the properties of the beads forming trimers at these values of λ are very close to water. For values larger than 0.5 all the included trimers are stably inside the micelle from the beginning to the end of the simulation. In Figure 10 the time behavior of L64 chains distributions inside the bilayer, assembled and free are reported for all systems with λ larger than 0.5 (0.6, 0.8, 0.9, 1.0). The plots of other systems are reported in the supporting information section. We observe that higher is the hydrophobicity and slower is the chain release process from the micelle to the water phase. In particular, for the systems at λ=0.16 and 0.20 the micelle dissolution process takes 1 and 2μs,

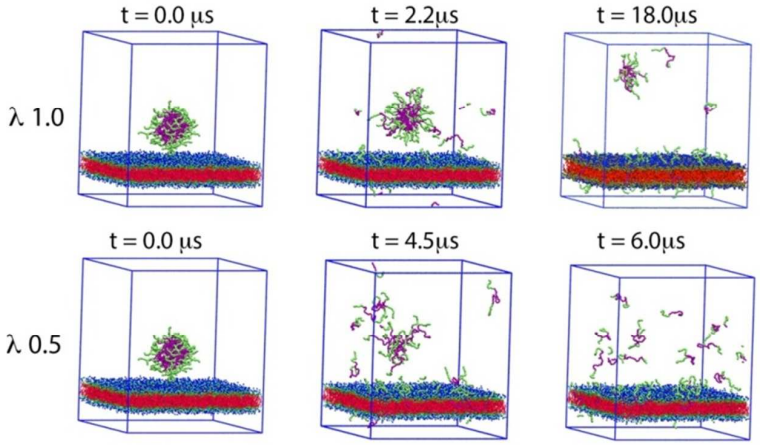

Fig.9 Snapshots of systems IV (258.072 coarse-grained beads corresponding to ~3.000.000 of atoms) at different values of λ having an L64 micelle in contact with DPPC lipid bilayer.

respectively. Differently, the systems having trimers with λ=0.5 take longer (between 4 and 5μs) to reach the equilibrium.

Micelles including trimers of larger hydrophobicity (λ from 0.6 to 1.0) take 8-12 μs, depending on the system, to reach equilibrium. After that time the micelles still remain stable and a slow process of chain repartition between water and lipid bilayer occurs.

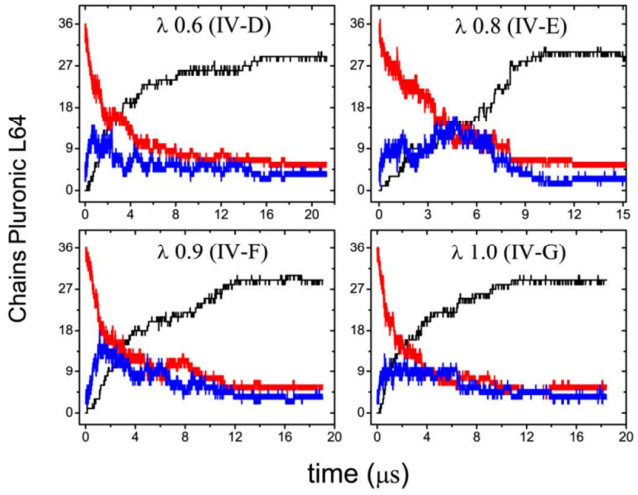

Fig.10 Time behaviour for systems IV D-G of L64 chains assembled as micelle (red curve), inside bilayer (black), in water (blue). For a complete definition of assembled, free and inside bilayer chains the reader can refer to the caption of **Figure 5**.

It is worth noting that an increase of hydrophobicity corresponds to an abrupt increase of the number of assembled chains. In particular, when going from λ=0.5 to λ=0.6, an increase in the micelle radius of about nine times can be obtained.

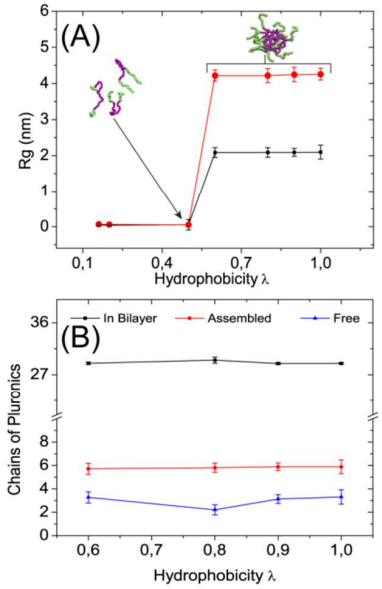

Fig.11 (A) Behavior of the radius of gyration of L64 micelle at different value of λ. Total radius (red curve), hydrophobic core radius (black curve). (B) Behavior of assembled (red curve), in bilayer (black curve) and free (blue curve) L64 chains as functions of hydrophobicity (λ) of encapsulated trimers.

Moreover, we observe that the number of assembled chains, for systems in which the micellar aggregate is present, does not change significantly (Figure 11B). A similar behavior is found for shape and size of the micellar aggregate, for which the radial density profiles have been calculated. In particular, for the system III, and systems IV-(D)-IV(G), the radial density profiles of the assembled chains in equilibrium together with IBU or trimer molecules (Figure 12) have been calculated. The radial density of chains when embedding IBU or the trimer molecules does not change significantly. In particular, for both hydrophilic EO blocks and hydrophobic PO block, only slight differences have been found (Figure 12A-B). As for the IBU and trimer molecules radial density, from the comparison of Figure 12C, we found that the distribution of IBU or trimer molecules inside the PO core is almost the same for all systems, but showing a slightly larger preference for the center of the micelle for both IBU molecules and trimers having λ=1.

In Figure 13 some of the density profiles of lipid bilayer have been reported. In particular we compared the density profiles of the system II (without IBU), system III (with IBU molecules inside micelle) and system IV-G (with trimer molecules having λ=1.0).

Such profiles have been calculated after that each system has reached the equilibrium state. From the plots we observe that the lipid bilayers do not show sensible differences of the profile. The distributions of the head and tails of the lipids are very close to each other and seem to be insensitive to the hydrophobicity. For the distribution of Pluronic chains inside the lipid bilayer we have the same behavior. (In the supporting information section all the density profiles of the others systems are reported).

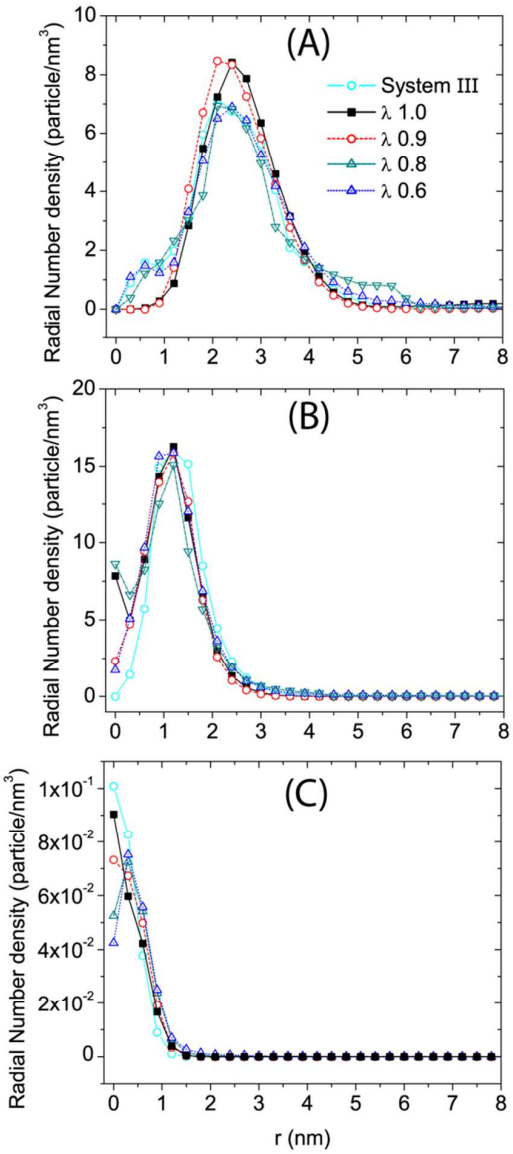

Fig.12 Radial density profile of: (A) EO blocks, (B) PO block, (C) IBU and trimer embedded molecules. Each profile is calculated with respect to the centre of the mass of IBU or trimer molecules. The profiles have been calculated from the data during the last 500.0 ns of the equilibrium state of each system.

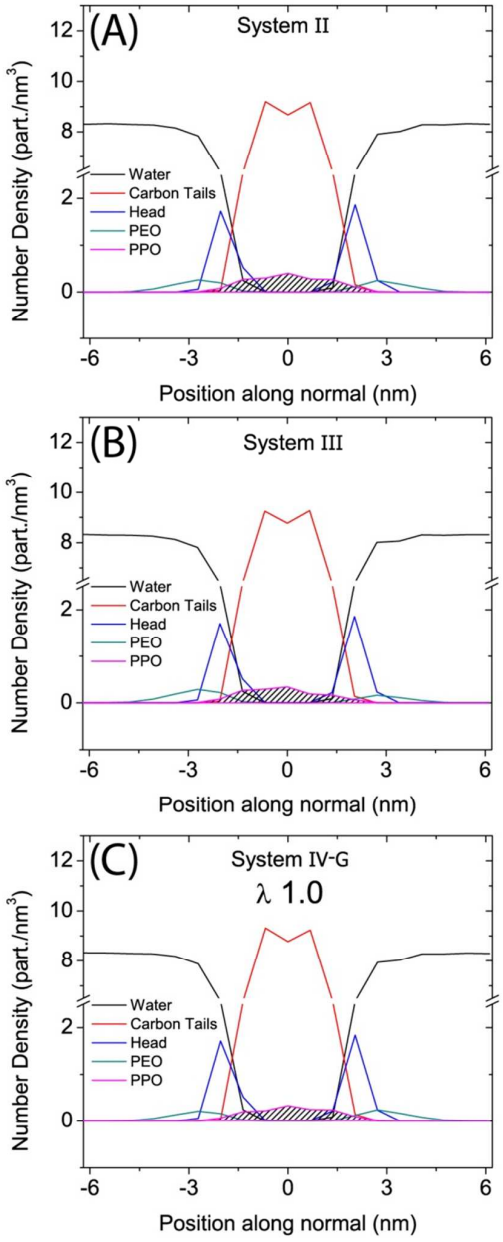

Fig.13 Number density profiles calculated for: (A) system II, (B) system III and (C) system IV-G with λ = 1.0. The density profiles have been calculated for the data during the last 500.0 ns of the equilibrium state of each system.

Conclusions

The development and validation of coarse-grained models of Pluronics that are able to describe micellar assemblies and their interactions with phospholipids have been reported. Molecular dynamics simulations of large-scale coarse-grained models (typically ~260.000 coarse-grained beads corresponding to ~3.000.000 of atoms) of Pluronic L64 block copolymers micelles interacting with lipid bilayers suitable to reach time (μs) and length (nm) scales relevant for the self assembly phenomena for

several systems have been reported. Simulations show, in agreement with several previous experiments, a release of triblock chains from the micelle inside the bilayer. This release changes the size of the micelles. The presence of a drug molecule inside the hydrophobic core of the micelle has a strong influence on this process. In particular, the micelle stability is a result of a complex interplay between drug/core and block-co-polymer/bilayer interactions modulating the structures of both micelle and bilayer. An interesting finding is that the micelle size shows an abrupt increase in a very narrow range of encapsulated molecule hydrophobicity. Changes in aggregate size and structure are critical in determining the mechanism of drug delivery from micellar structures. According to the paradigm of EPR effect, the understanding of the physico-chemical mechanism of the drug vector size and the important role of drug micelle interactions in it, are fundamental to improve the design of systems for cancer therapy. The models presented in this study are not generic, but still very close to atomistic ones and are able to represent specific molecular architectures. This important feature opens the way to a detailed understanding of the molecular mechanisms underlying the drug delivery processes.

Table 1 Force field bond parameters

Bond type	l_0 (nm)	K_{bond} (kJ mol^{-1}nm^{-2})
N-P	0.470	1250.0
P-G	0.470	1250.0
G-G	0.370	1250.0
G-C	0.470	1250.0
C-C[a]	0.470	1250.0
EO-EO	0.280	8000.0
PO-PO	0.280	5000.0
EO-PO	0.280	6500.0
E-B	0.310	7500.0
B-B	0.270	8000.0
B-C	0.310	7500.0

[a] These parameters have been used also for trimer model.

Table 2 Force field angle parameters

Angle type	θ (deg)	K_θ (kJ mol^{-1})
P-G-G	120.0	25.0
P-G-C	180.0	25.0
G-C-C	180.0	25.0
C-C-C	180.0	25.0
EO-EO-EO	155.0	40.0
EO-PO-PO	140.0	40.0
EO-EO-PO[a]	140.0	30.0
PO-PO-PO	140.0	40.0
E-B-B	150.0	50.0
B-B-B	120.0	50.0
B-B-C	150.0	50.0

[a] These parameters have been used also for trimer model.

Table 3. Particle-field interaction matrix. χ_{AB}·RT(kJ mol^{-1}) for Systems I-III.

	N	P	G	C	Water	EO	PO
N	0.00	-1.50	6.30	9.0	-8.10	-5.25	2.60
P	-1.50	0.00	4.50	13.50	-3.60	-0.75	7.55
G	6.30	4.50	0.00	6.30	4.50	5.00	0.00
C[a]	9.00	13.50	6.30	0.00	33.75	7.80	-1.60
Water	-8.10	-3.60	4.50	33.75	0.00	1.50	4.60
EO[b]	-5.25	-0.75	5.00	7.89	1.50	0.00	16.00
PO	2.60	7.55	0.00	-1.60	4.60	16.00	0.00

a) same parameters have been used for the particle of type B of IBU molecules. b) same parameters for particle of type E of IBU molecules

Table 4. Particle-field interaction matrix. χ_{AB}·RT(kJ mol^{-1}) for Systems IV.

λ	N	P	G	C	Water	EO	PO
1.00	9.00	13.50	6.30	0.00	33.75	7.80	-1.60
0.90	7.28	11.79	6.12	3.37	30.37	7.22	-0.98
0.80	5.57	10.80	5.94	7.75	27.00	6.64	-0.36
0.60	2.14	6.66	5.58	13.50	20.25	5.84	0.88
0.50	0.43	4.95	5.40	16.87	16.87	4.90	1.50
0.20	-4.70	-0.18	4.86	27.00	6.75	3.16	3.61
0.16	-5.39	-0.86	4.79	28.35	5.40	2.93	3.61

Table 5. Composition of systems used for the CMC calculation.[a]

System	Composition				Box Size
	no. L64	no. Water	no. Particles	mM	(nm)
A	19	223264	224328	1.122	30x30x30
B	9	223824	224328	0.532	30x30x30
C	6	223992	224328	0.354	30x30x30
D	5	224048	224328	0.295	30x30x30
E	4	224104	224328	0.236	30x30x30

[a]The experimental value of CMC reported by Alexandridis[45] is 0.344mM at 313 K.

Table 6. Simulated Systems

Systems	Composition (no. of molecules)					Box size (nm)	Simulated time (μs)
	L64	Water	DPPC	Embedded Molecule	Particle no.		
I	38	222200	0	0	224328	30x30x30	6
II	38	222200	2812	0	258072	30x30x34	5
III[a]	38	222200	2812	5	258097	30x30x34	13
IV-A[b]	38	222200	2812	8	258096	30x30x34	5
IV-B[b]	38	222200	2812	8	258096	30x30x34	5
IV-C[b]	38	222200	2812	8	258096	30x30x34	6
IV-D[b]	38	222200	2812	8	258096	30x30x34	21
IV-E[b]	38	222200	2812	8	258096	30x30x34	15
IV-F[b]	38	222200	2812	8	258096	30x30x34	18
IV-G[b]	38	222200	2812	8	258096	30x30x34	18

[a]Embedded molecules used for this system are Ibuprofen. [b]SystemsIV having embedded trimers of increasing hydrophobicity λ ranging from 0.16 (IV-A) to 1 (IV-G).

Acknowledgments

G.M. and D. R. thank Deutschen Forschungsgemeinschaft (DFG) for funding in the framework of the project ‘‘The study of detailed mechanism of polymers/biological membrane interactions using computer simulation’’ (RO 3571/3-1).

G. M. thanks MIUR (PRIN2008 and FIRB ‘‘RETE ITAL- NANONET’’) for financial support. Moerover, G.M. thanks the European Soft Matter

Infrastructure (ESMI) and Forschungszentrum Juelich team for the HPC facilities (www. fz-juelich.de).

Notes and references

[a] *Dipartimento di Chimica e Biologia, Università di Salerno,I-84984 via Ponte don Melillo, Fisciano(SA), Italy*
[b] *IMAST Scarl-Technological District in Polymer and Composite Engineering, P.le Bovio 22, 80133 Napoli (NA), Italy*
[c] *Jacobs University Bremen, Campus Ring 1, D-28759 Bremen, Germany*
[d] *Institute of Nano-photonics, School of Physics and Material Engineering, Dalian Nationalities University, Dalian 116600, China*
[e] *Department of Physics, Tohoku University, Aoba, Aoba-ku, Sendai 980-8578, Japan*
* *e-mail: gmilano@unisa.it*

† Electronic Supplementary Information (ESI) available: [details of any supplementary information available should be included here]. See DOI: 10.1039/b000000x/

‡ Footnotes should appear here. These might include comments relevant to but not central to the matter under discussion, limited experimental and spectral data, and crystallographic data.

1. R. Duncan and R. Gaspar, *Molecular Pharmaceutics*, 2011, **8**, 2101-2141.
2. R. Duncan, *Current Opinion in Biotechnology*, 2011, **22**, 492-501.
3. R. Duncan, *Nat. Rev. Drug Discovery*, 2003, **2**, 347.
4. R. Duncan, *Nat. Rev. Cancer*, 2006, **6**, 688.
5. G. Pasut and F. M. Varonese, *Adv. Drug Delivery Rev.*, 2009, **61**, 1177.
6. Y. Matsumura, *Adv. Drug Delivery Rev.*, 2008, **60**, 899.
7. Y. Matsumura and K. Kataoka, *Cancer Sci.*, 2009, **100**, 572.
8. D. Farrel, K. Ptak, N. J. Panaro and P. Grodzinski, *Pharmaceutical research*, 2011, **28**, 273.
9. T. M. Allen, *Nat. Rev. Drug Discovery*, 2002, **2**, 750-763.
10. V. P. Torchilin, *Nat. Rev. Drug Discovery*, 2005, **4**, 145.
11. W. C. Zamboni, *Clin. Cancer Res.*, 2005, **11**, 8230.
12. K. K. Upadhyay, H. G. Agrawal, C. Upadhyay, C. Schatz, J. F. Le Meins, A. Misra and S. Lecommandoux, *Crit. Rev. Ther Drug Carrier Syst.*, 2009, **26**, 157.
13. A. B. Kabanov, E. V. Batrakova and V. Y. Alakhov, *Adv. Drug Delivery Rev.*, 2002, **54**, 759.
14. Y. Matsumura and H. Maeda, *Cancer Res.*, 1986, **6**, 6387.
15. A. B. Kabanov, V. P. Chekhonin, V. Alakhov, E. V. Batrakova, A. S. Lebedev, N. S. Melik-Nubarov, S. A. Arzhakov, A. V. Levashov, G. V. Morozov and E. S. Severin, *FEBS Lett.*, 1989, **258**, 343.
16. V. Y. Alakhov and A. V. Kabanov, *Expert Opin. Investing. Drugs*, 1998, **7**, 1453-1473.
17. A. A. Exner, T. M. Krupka, K. Sherrer and J. M. Teets, *J. Control. Release* 2005, **106**, 188.
18. M. Hans, K. Shimoni, D. Danino, S. J. Siegel and A. Lowman, *Biomacromolecules*, 2005, **6**, 2708.
19. V. Alakhov, E. Klinski, S. Li, G. Pietrzynski, A. Venne, E. Batrakova, T. Bronitch and A. Kabanov, *Colloids and Surfaces B: Biointerfaces*, 1999, **16**, 113-134.
20. S. Pal, G. Milano and D. Roccatano, *Journal of Physical Chemistry B*, 2006, **110**, 26170-26179.
21. S. Nawaz, M. Redhead, G. Mantovani, C. Alexander, C. Bosquillon and P. Carbone, *Soft Matter*, 2012, **8**, 6744-6754.
22. M. Redhead, G. Mantovani, S. Nawaz, P. Carbone, D. C. Gorecki, C. Alexander and C. Bosquillon, *Pharmaceutical research*, 2012, **29**, 1908-1918.
23. S. Samanta, S. Hezaveh, G. Milano and D. Roccatano, *The Journal of Physical Chemistry B*, 2012, **116**, 9286-9286.
24. S. Samanta, S. Hezaveh, G. Milano and D. Roccatano, *The Journal of Physical Chemistry B*, 2012, **116**, 5141-5151.
25. S. Hezaveh, S. Samanta, A. De Nicola, G. Milano and D. Roccatano, *The Journal of Physical Chemistry B*, 2012, **116**, 14333-14345.
26. P. F. J. Fuchs, H. S. Hansen, P. H. Huenenberger and B. A. C. Horta, *Journal Of Chemical Theory And Computation*, 2012, **8**, 3943-3963.
27. S. Hezaveh, S. Samanta, G. Milano and D. Roccatano, *J. Chem. Phys.*, 2012, **136**, 124901.
28. S. Hezaveh, S. Samanta, G. Milano and D. Roccatano, *J. Chem. Phys.*, 2011, **135**, 16450.
29. K. M. Langner and G. J. A. Sevink, *Soft Matter*, 2012, **8**, 5102-5118.
30. M. Mueller, K. Katasov and M. Schick, *Physics Reports*, 2006, **434**, 113-176.
31. M. Giuseppe, K. Toshihiro and N. Antonio De, *Physical Biology*, 2013, **10**, 045007.
32. M. Homberg and M. Muller, *The Journal of Chemical Physics*, 2010, **132**, 155104-155118.
33. G. J. A. Sevink, M. Charlaganov and J. G. E. M. Fraaije, *Soft Matter*, 2013, **9**, 2816-2831.
34. K. C. Daoulas and M. Muller, *J. Chem. Phys.*, 2006, **125**.
35. K. C. Daoulas, M. Muller, J. J. de Pablo, P. F. Nealey and G. D. Smith, *Soft Matter*, 2006, **2**, 573-583.
36. G. Milano and T. Kawakatsu, *Journal of Chemical Physics*, 2009, **130**, 214106.
37. G. Milano and T. Kawakatsu, *Journal of Chemical Physics*, 2010, **133**, 214102.
38. A. De Nicola, Y. Zhao, T. Kawakatsu, D. Roccatano and G. Milano, *Journal of Chemical Theory and Computation*, 2011, **7**, 2947-2962.
39. A. De Nicola, Y. Zhao, T. Kawakatsu, D. Roccatano and G. Milano, *Theoretical Chemistry Accounts*, 2012, **131**, 1167.
40. A. De Nicola, G. Milano and T. Kawakatsu *Macromolecular Chemistry and Physics*, 2013, **214**, 1940-1950.
41. Y. Zhao, A. De Nicola, T. Kawakatsu and G. Milano, *Journal of Computational Chemistry*, 2012, **33**, 868-880.
42. X. Cao, G. Xu, Y. Li and Z. Zhang, *The Journal of Physical Chemistry A*, 2005, **109**, 10418-10423.
43. R. D. Groot and P. B. Warren, *The Journal of Chemical Physics*, 1997, **107**, 4423-4435.
44. L. Yang, P. Alexandridis, D. C. Steytler, M. J. Kositza and J. F. Holzwarth, *Langmuir*, 2000, **16**, 8555-8561.
45. P. Alexandridis, J. F. Holzwarth and T. A. Hatton, *Macromolecules*, 1994, **27**, 2414-2425.
46. G. Pembouong, N. Morellet, T. Kral, M. Hof, D. Scherman, M.-F. Bureau and N. Mignet, *Journal of Controlled Release*, 2011, **151**, 57-64.

47. M. A. Firestone and S. Seifert, *Biomacromolecules*, 2005, **6**, 2678-2687.
48. M. A. Firestone, A. C. Wolf and S. Seifert, *Biomacromolecules*, 2003, **4**, 1539-1549.
49. D. Fritz, K. Koschke, V. A. Harmandaris, N. F. van der Vegt and K. Kremer, *Phys Chem Chem Phys*, 2011, **13**, 10412-10420.
50. B. Foster, T. Cosgrove and B. Hammouda, *Langmuir*, 2009, **25**, 6760-6766.

Supporting Information

Micellar Drug Nanocarriers and Biomembranes: How do they Interact?

Antonio De Nicola,[a,b] *Samira Hezaveh,*[c] *Ying Zhao,*[d] *Toshihiro Kawakatsu,*[e] *Danilo Roccatano,*[c] *and Giuseppe Milano,*[*a,b]

[a]Dipartimento di Chimica e Biologia, Università di Salerno, I-84084 via Ponte don Melillo Fisciano (SA), Italy

[b]IMAST Scarl-Technological District in Polymer and Composite Engineering, P.le Bovio 22, 80133 Napoli (NA), Italy

[c]Jacobs University Bremen, Campus Ring 1, D-28759 Bremen, Germany

[d]Institute of Nano-photonics, School of Physics and Materials Engineering, Dalian Nationalities University, Dalian 116600, China

[e]Department of Physics, Tohoku University, Aoba, Aramaki, Aoba-ku, Sendai 980-8578, Japan

*e-mail: gmilano@unisa.it

Models and parameters

The initial set of χ paramaters for the interaction between polyethylen oxide (EO) and polypropylene oxide (PO) with phospholipid bilayer hase been obtained from a DPD study of Groot[1]. The refinement of these parameters has been based on the reproduction of electron density profile of correspondig atomistic simulations of 1,2-dimethoxyethane (DME) and 1,2-dimetoxypropane (DMP) reported in reference[2]. The electron density profiles reported in **Figure S1** have been calculated averaging on the last 150 ns of each trajectory. The composition of the systems used for the parametrization is reported in **Table 1**. The resulting χ parameters interaction matrix of the CG model are reported in **Table 2**.

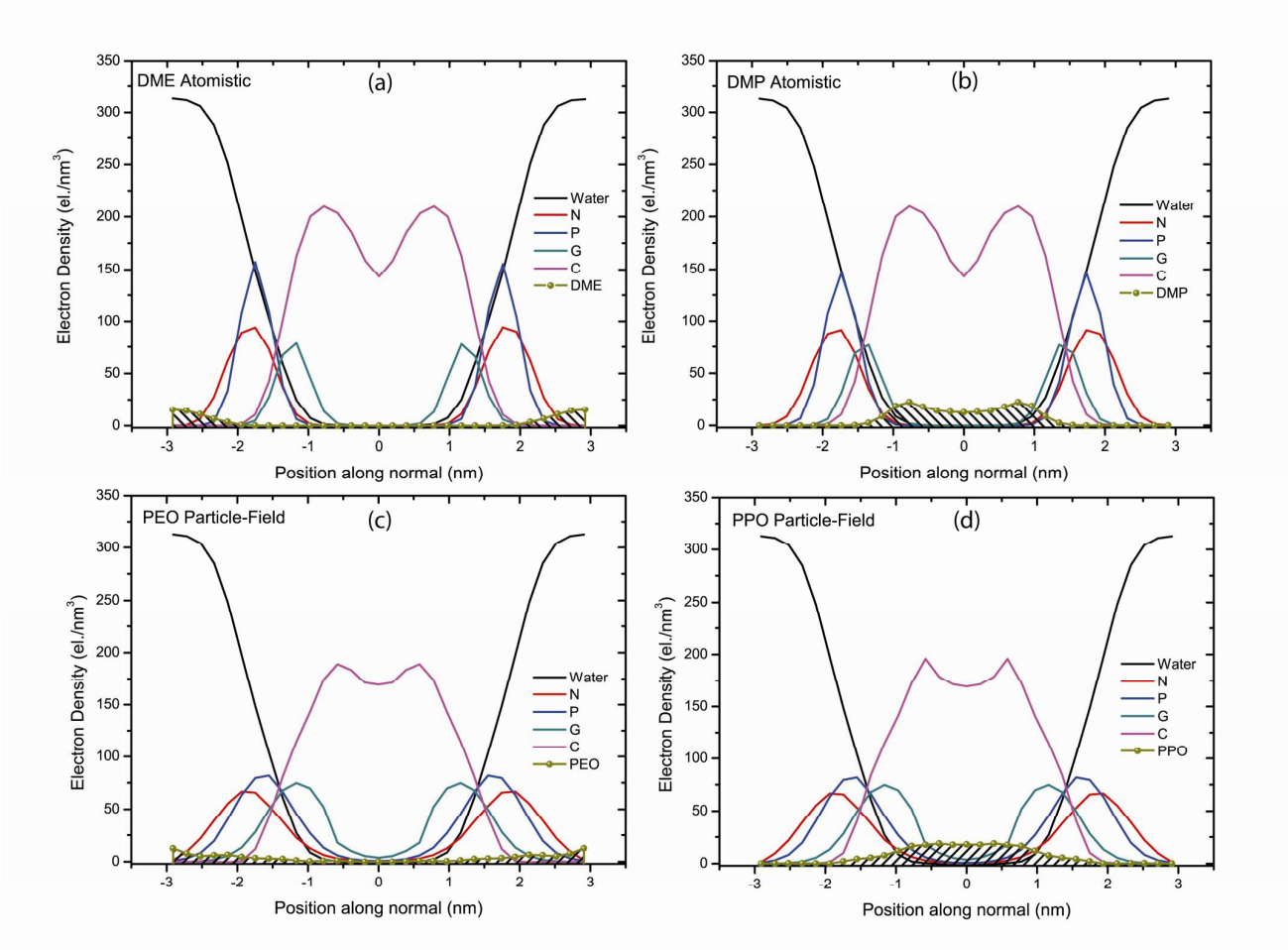

Figure S1 Electron density profiles of : (a) System of 1,2-dimethoxyethane in lipid/water mixture. (b) System of 1,2-dimethoxypropane in lipid/water mixture. (c) Sytem of EO trimers in lipid water mixture. (d) System of PO trimers in lipid/water mixture.

Table 1. Composition of Systems.

System	Composition (no. Particles)			Box size
	DMPC	Oligomer	no. of Water	(nm)
a	128	1 DME	7962	6.34x6.34x9.69
b	128	1 DMP	7958	6.43x6.43x9.40
c	128	1 PEO	1990*	6.34x6.34x9.69
d	128	1 PPO	1989*	6.43x6.43x9.40

*The values reported as no. of Water are relative to CG water beads. One water bead correspond to four real water molecules.

Table 2. Particle-field interaction matrix. $\chi_{AB} \times RT$(kJ mol^{-1}).

Bead type	N	P	G	C	Water	EO	PO
N	0.00	-1.50	6.30	9.0	-8.10	-5.25	2.60
P	-1.50	0.00	4.50	13.50	-3.60	-0.75	7.55
G	6.30	4.50	0.00	6.30	4.50	5.00	0.00
C	9.00	13.50	6.30	0.00	33.75	7.80	-1.60
Water	-8.10	-3.60	4.50	33.75	0.00	1.50	4.60
EO	-5.25	-0.75	5.00	7.89	1.50	0.00	16.00
PO	2.60	7.55	0.00	-1.60	4.60	16.00	0.00

Critical Micelle Concentration (CMC) of Pluronics Model

We investigate the CMC of the model considering the stability of the micelle aggregate as function of the concentration of L64 in water. In particular 5 different concentrations have been considered. The composition of such systems is reported in **Table 3**. For each system we calculate the distribution of free and assembled chains, according to the number of neighbouring chains (zero neighbouring are considered free chains). The number of neighbors is calculated on the basis of cut off criteria (1 nm) on the shorter distance between PO units of two different chains. In **Figure S2** the time behavior of the fraction of assembled L64 chains is reported. We found that the CMC of the proposed model is in an interval ranging from 0.532 to 0.354 mM. This interval is very close to the experimental CMC value of 0.344 mM at 313K reported by Alexandridis[3].

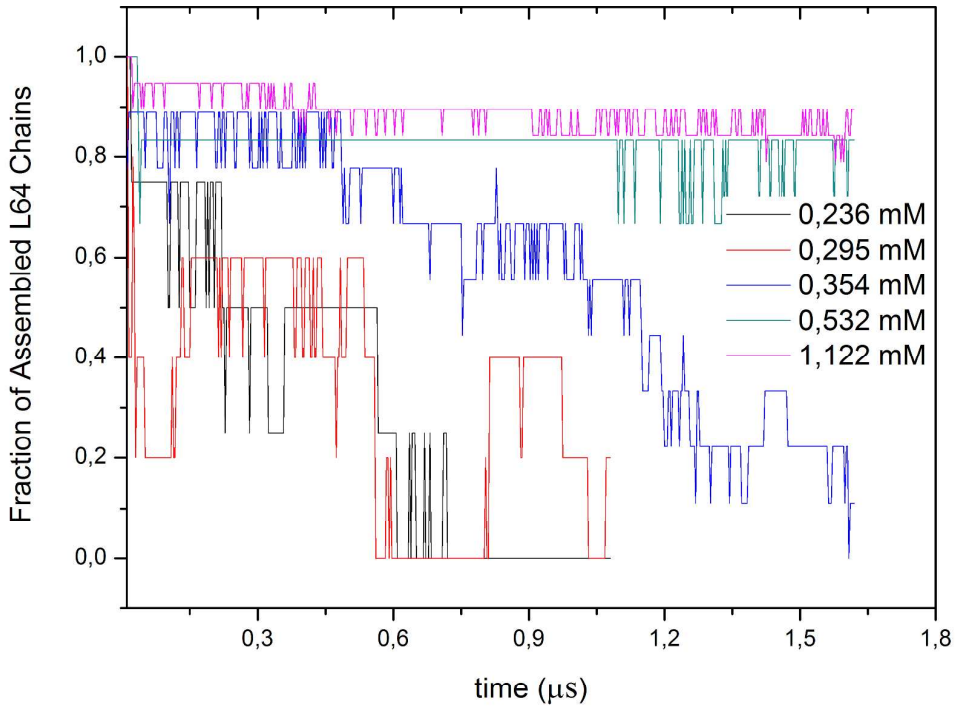

Figure S2 Time behavior of fraction of assembled L64 chains at different concentrations.

Table 3 Composition of systems used for the CMC calculation.

System	Composition			Box Size	
	no. L64	no. Water	no. Particles	mM	(nm)
A	19	223264	224328	1.122	30.0 x 30.0 x30.0
B	9	223824	224328	0.532	30.0 x 30.0 x 30.0
C	6	223992	224328	0.354	30.0 x 30.0 x 30.0
D	5	224048	224328	0.295	30.0 x 30.0 x 30.0
E	4	224104	224328	0.236	30.0 x 30.0 x 30.0

*The values reported as no. of Water are relative to CG water beads. One water bead correspond to four real water molecules.

Supplementary Results

Aggregation Number

Experimentally the micelle number of aggregation ($N_{agg.}$) for a system of Pluronic L64 at 2.5 wt% is 38 (at 313 K)[4]. In order to understand the behavior of our model respect to the number of aggregation, we performed 5 simulations (a-e) of a single micelle in water with increasing number of L64 chains, starting from 38 up to 53. Moreover, we fixed the concentration of these systems at 2.5 wt%. The composition of the simulated systems is reported in **Table 4**.

In **Figure S3** we report the occurrence frequency versus the cluster size at different time. The plot in **Figure S3-(a)** is relative to the system of the micelle made by 38 chains of L64. It is clear that $N_{agg.}$ is strictly close to 38. Increasing the number of L64 chains constituting the micelle, we observe a broader distribution cluster size respect to the reference system (a). In addition, we report in **Figure S4** also the time behavior of cluster size for the systems (a-e).

Table 4 System composition relative at the figure S4.

System	Composition				Box size	Simulated time
	no. of L64	no. of Water	no. Particle	Conc. wt%	(nm)	(μs)
a	38	54733	56861	2.5	18.0x18.0x18.0	4.2
b	41	59095	61391	2.5	18.4x18.4x18.4	4.2
c	45	64861	67381	2.5	18.9x18.9x18.9	4.2
d	48	69185	71873	2.5	19.4x19.4x19.4	4.2
e	53	76444	79359	2.5	20.1x20.1x20.1	4.2

*The values reported as no. of Water are relative to CG water beads. One water bead correspond to four real water molecules.

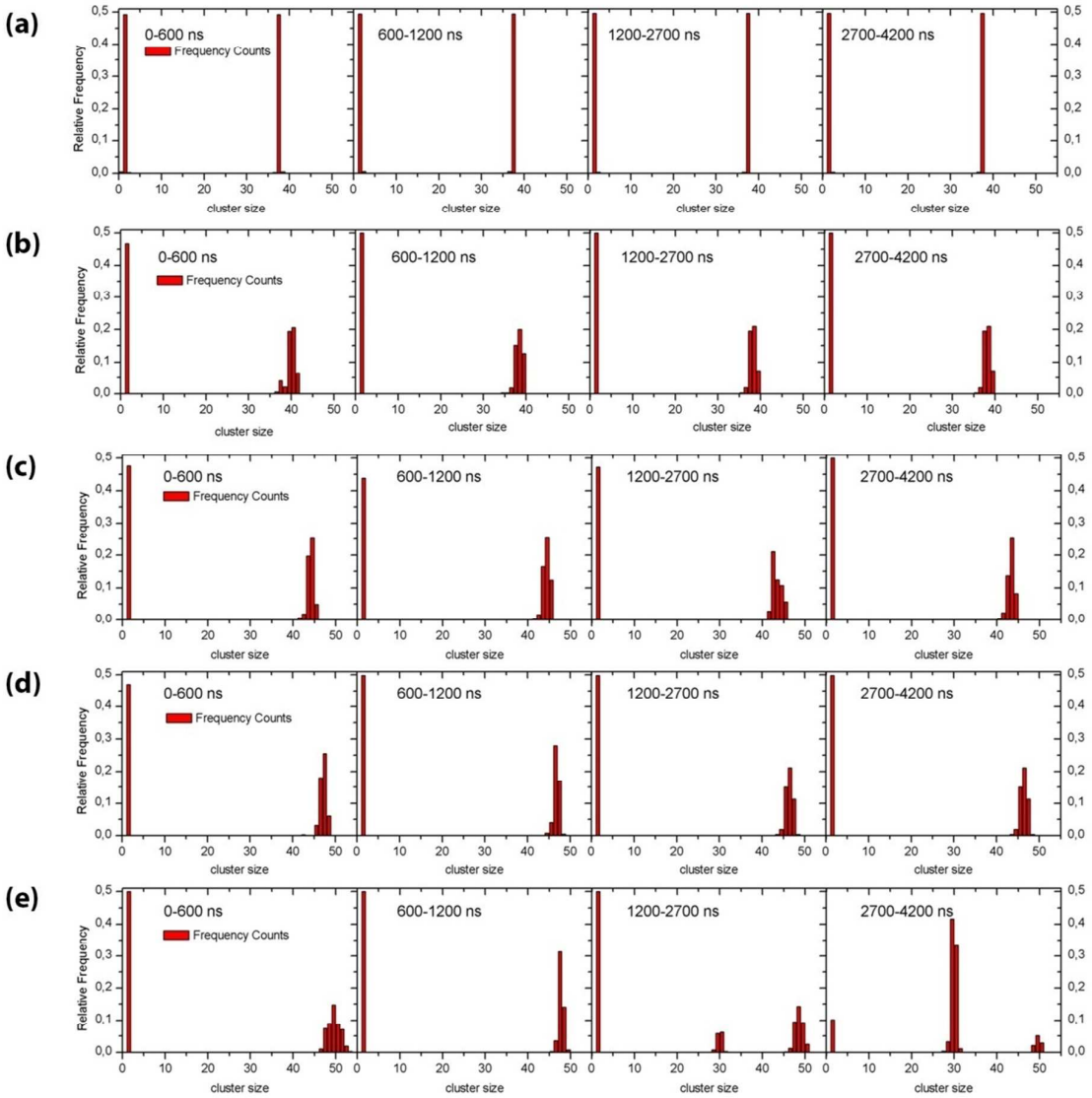

Figure S3 Frequency of occurrence of clusters of different size for systems a-e.

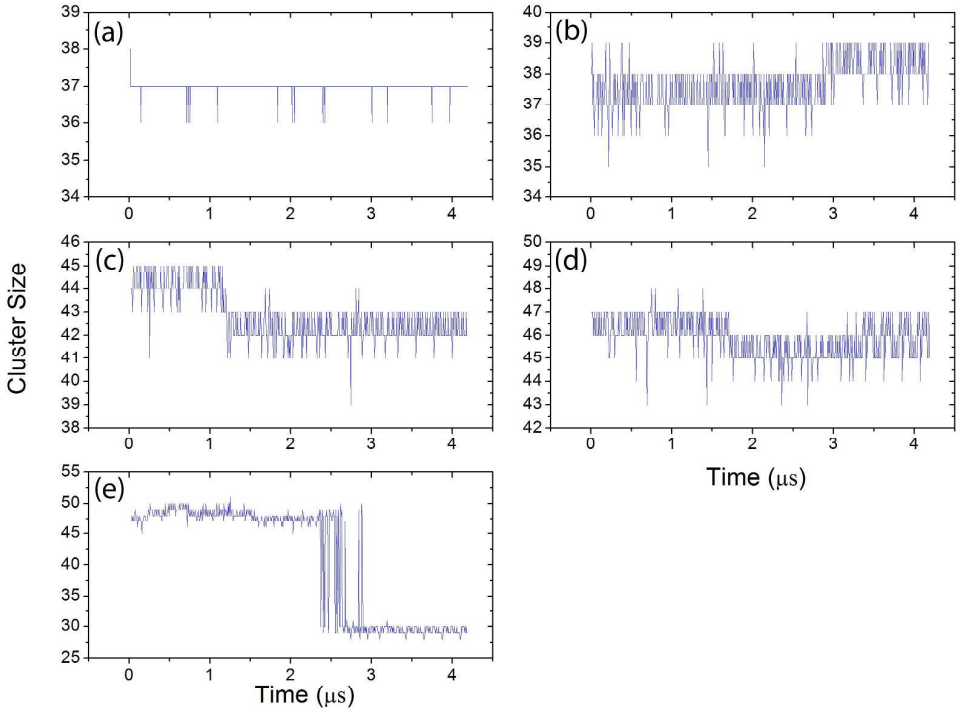

Figure S4 Time behavior of cluster size for the systems (a-e).

Validation of single trajectory behavior

In order to validate simulation results, three different independent simulations of the system III have been performed. In **Figure S5** block averages of three possible L64 chains states as function of time (inserted into bilayer, assembled and free; for a quantitative definition of these states the reader can refer to the caption of Figure 5 of the paper) are shown. The main behavior in all three cases is very similar and at equilibrium the chain distributions converge to similar values. Each point on the plot represents the time block average calculated using a time interval of 1.0 μs. In addition, in **Figure S6** the instantaneous time behavior of three independent simulations of the system III, jointly with average time behavior, is reported. From the **Figure S6** it is clear that the instantaneous behavior of a single simulation is representative of the whole process.

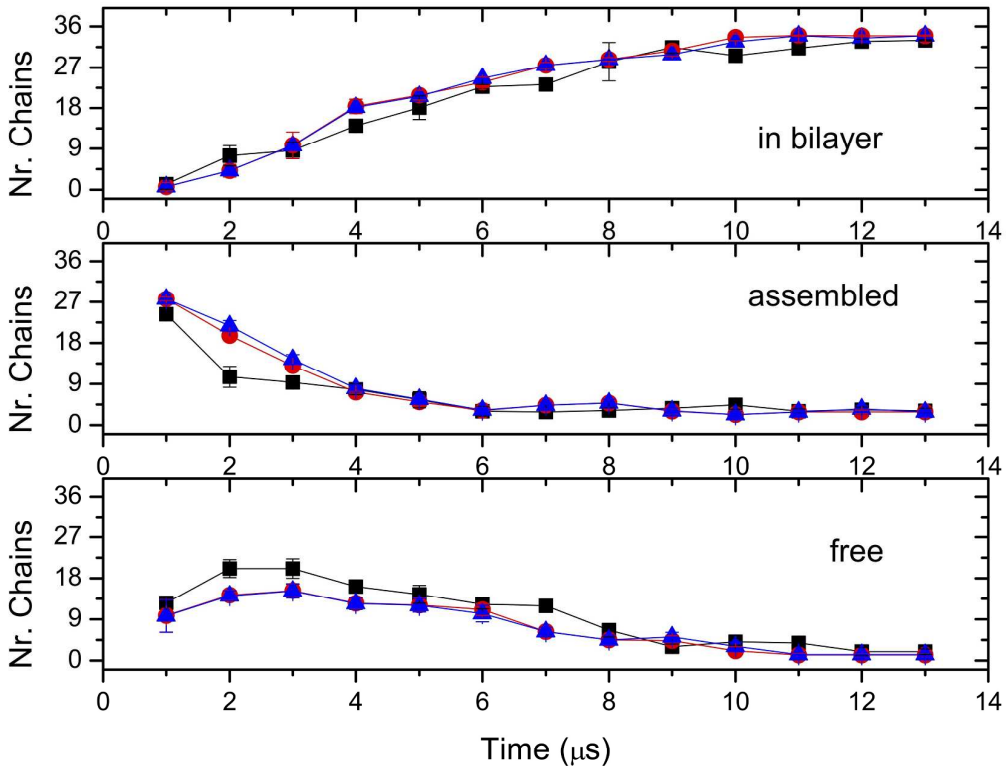

Figure S5 Time behavior of L64 chains in bilayer (top), assembled (middle) and free (bottom). Each point is a time average over 1.0 μs. Three different simulations of the system III have been used for the block average calculation (for the composition of the system III refer to table 6 of the paper).

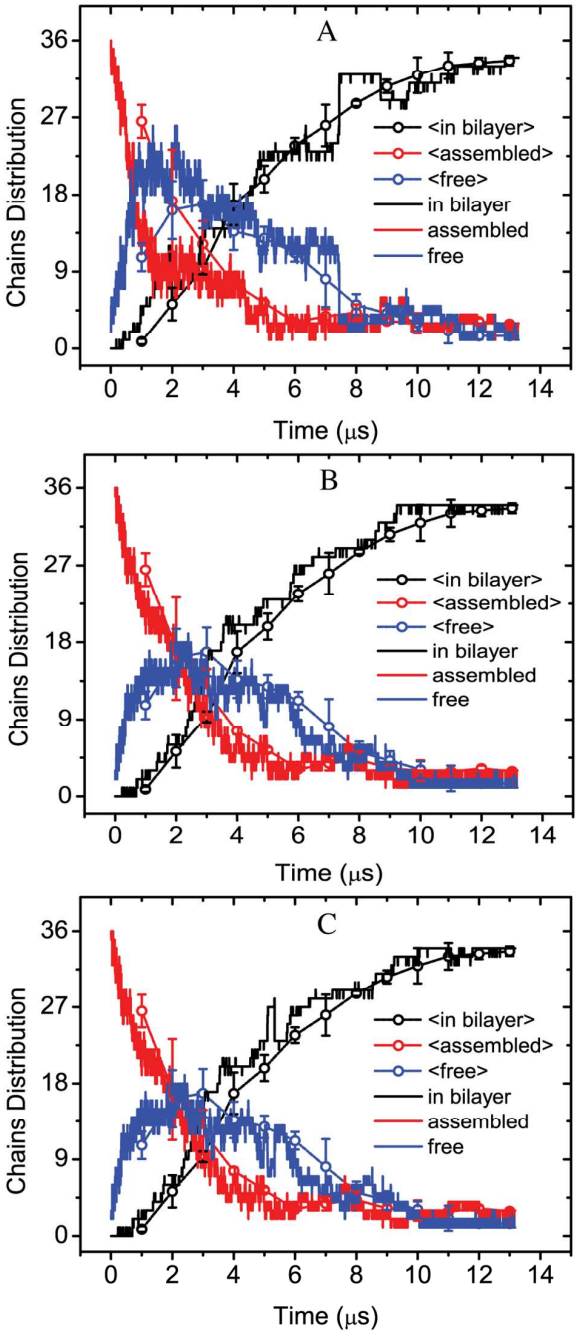
A
B
C
Chains Distribution
Time (μs)
<in bilayer>
<assembled>
<free>
in bilayer
assembled
free
0
9
18
27
36
0
2
4
6
8
10
12
14

Figure S6 Instantaneous behavior of three independent simulations (A,B,C) for the system III. The symbols represent the averages over 1.0 μs of each state of the chains (in bilayer, assembled and free).

The comparison between the equilibrium values of the micelle radius calculated using three independent simulations of the system III is repoted, jointly with the related table, below.

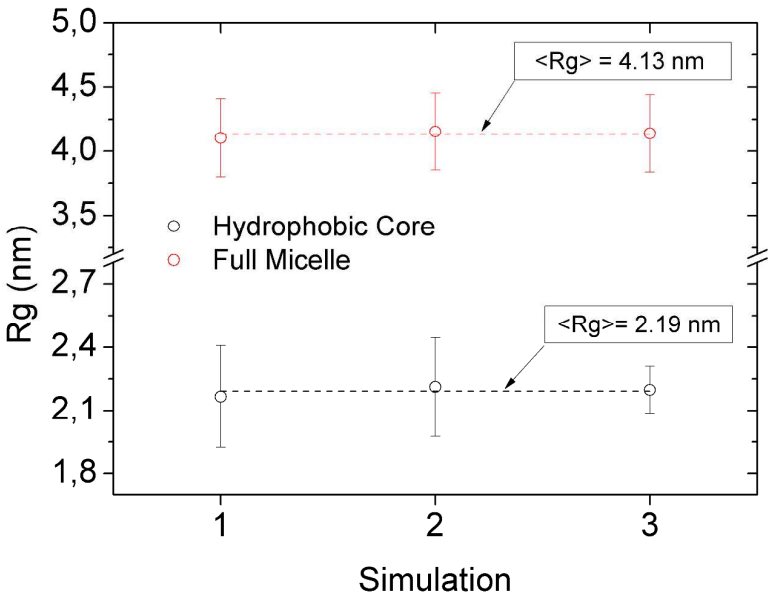

Figure S7 Radii of gyration of the hydrophobic core and full micelle calculated for three different simulation of the system III. Each point represent the time average over the last 1.0 μs of the each simulation.

Table 5 Radii of gyration calculated for three different simulation of the system III

Simulation	**Radius of gyration** (nm)			
	Hydrophobic Core	Standard Deviation %	Full Micelle	Standard Deviation %
1	2.17	6.3	4.10	8.0
2	2.21	6.1	4.15	7.9
3	2.20	2.9	4.14	7.9

Timescale Connection

Ideally, the exchange process of L64 chains between the micelle and the lipid bilayer, as discussed in the paper, can be divided in three elementary processes. In particular, we can consider three processes: Pluronic chain detachment from the micelle, chain diffusion in water, and chain insertion into the lipid bilayer. Reasonably, the diffusion process is the slowest and the governing the rate of the observed process. To better evaluate the time scales involved in such global process, a more systematic study has been done.
We performed three independent simulations similar to the one reported in Figure 6 of the main paper. In particular, we evaluated the velocity of L64 chain insertion in the following way. The time behavior of z component (perpendicular to the bilayer plane) of the distance between the geometrical center of the PPO block and the center of mass of the particles of type C (hydrophobic sector of the lipid bilayer) has been considered. In the figure below, the time behavior of this distance is reported. In order to estimate the velocity of this process the time behavior has been fitted with a sigmoidal function of the type:

$$z(t) = \frac{z_1 - z_2}{1 + e^{(t-t_0)/\delta t}} + z_2$$

The velocity of insertion can be estimated by considering the value of the first derivative at t_0 $z'(t_0) = \frac{z_2 - z_1}{4\delta t}$ as indicated in the figure below.

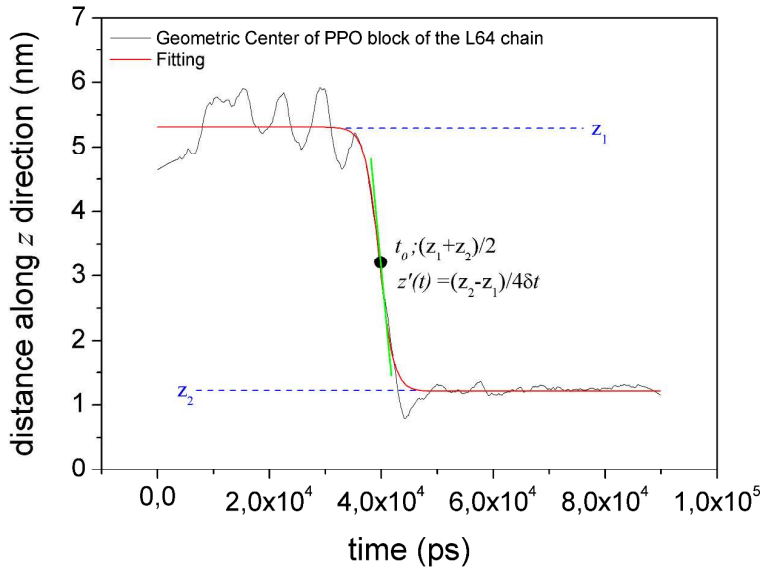

Figure S8 Time behavior of z component of the distance between geometric center of PPO block and center of mass of hydrophobic sector of the lipid bilayer during the insertion process of a single L64 chain (black curve). In red is reported the fitting obtained using a sigmoidal function defined with the equation above.

In the Table 6 the fitted velocities for three independent particle-particle and particle-field simulations are reported.

Table 6 Estimated insertion velocities for particle-particle and particle-field simulations

Simulation	(Particle-Particle) [nm/ps] 10^4	(Particle-Field) [nm/ps] 10^4
1	1.7 ± 0.2	2.9 ± 0.2
2	7.8 ± 0.3	2.6 ± 0.3
3	5.5 ± 0.4	5.6 ± 0.3

From the values reported in the table above it is clear that the process of chain insertion is fast (takes about 8-10 ns) and it has similar velocities for both particle-particle and particle field simulations.
According to these results we can reasonably conclude that the slowest process governing the chain exchange process between the micelle and the bilayer is the diffusion of L64 chains. In this way a reasonable estimate of the scaling factor could be the ratio between diffusion coefficients of particle-particle and particle-field simulations (a factor 15).

The time behavior of chain distribution of the systems IV-(A,C) are reported in **Figure S9**. For the composition of such systems refer to table 6 of the paper.

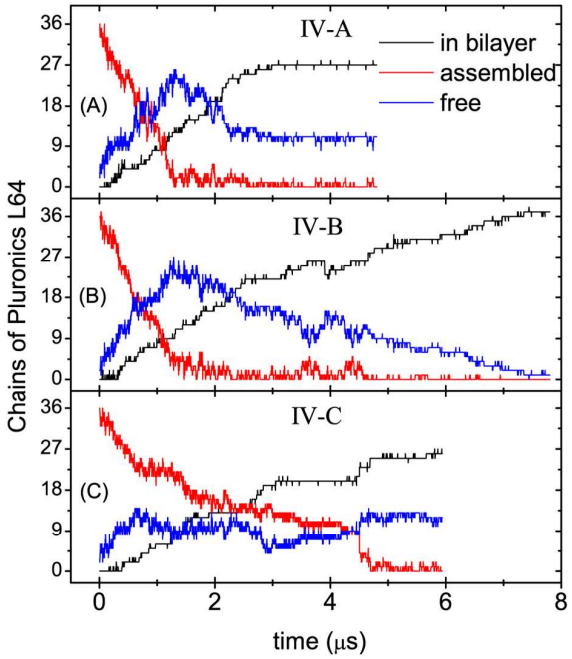

Figure S9 Time behaviour for systems IV-A,C (corresponding to systems with λ 0.16, 0.20 and 0.5) of L64 chains assembled as micelle (red curve), inside bilayer (black), in water (blue). The L64 chains, for a given configuration, are counted as inside bilayer if the last one PO bead is located between the average heighest of upper and lower lipid layers. The remaning chains are counted as free or assembled according to the number of neighboring chains (zero neighboring are considered free chains). The number of neighbors is calculated on the basis of a cut off criteria (1 nm) on the shortest distance between PO units of two different L64 chains.

The number density profiles of systems IV-(D-E-F) are reported in **Figure S10**. The last 0.5 μs of the equilibrium state of each simulation have been considered in the calculation of profiles.

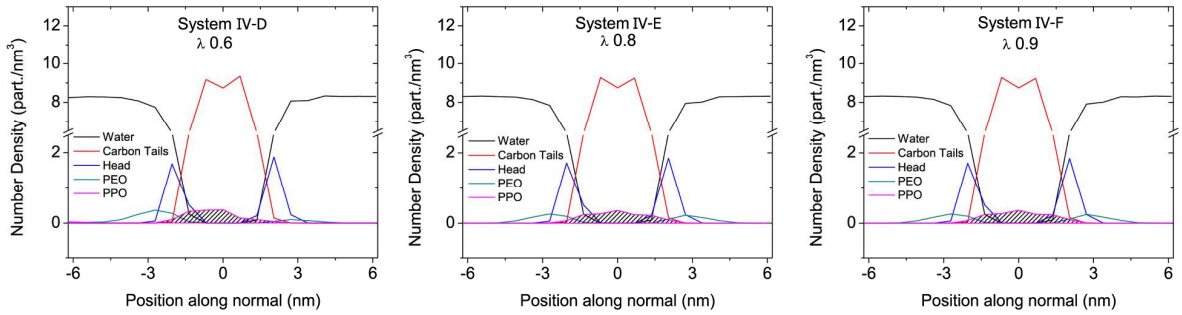

Figure S10 Number density profile of the systems IV-(D-E-F). We consider as lipid head the group of CG beads formed by N, P and g type. The carbon tails are counted as a single group of type C particles. For the particles type definition refer to the Figure 2 of the paper.

References

1. R. D. Groot and P. B. Warren, *The Journal of Chemical Physics*, 1997, **107**, 4423-4435.

2. S. Hezaveh, S. Samanta, G. Milano and D. Roccatano, *J. Chem. Phys.*, 2011, **135**, 16450.

3. P. Alexandridis, J. F. Holzwarth and T. A. Hatton, *Macromolecules*, 1994, **27**, 2414-2425

4. L. Yang, P. Alexandridis, D. C. Steytler, M. J. Kositza and J. F. Holzwarth, *Langmuir*, 2000, **16**, 8555-8561.